A New Regime for Operating Capacitive Micromachined Ultrasonic Transducers

Baris Bayram, Edward Hæggström, Goksen G. Yaralioglu, *Member, IEEE*, and Butrus T. Khuri-Yakub, *Fellow, IEEE*

***Abstract*—We report on a new operation regime for capacitive micromachined ultrasonic transducers (cMUTs). Traditionally, cMUTs are operated at a bias voltage lower than the collapse voltage of their membranes. In the new proposed operation regime, first the cMUT is biased past the collapse voltage. Second, the bias voltage applied to the collapsed membrane is reduced without releasing the membrane. Third, the cMUT is excited with an ac signal at the bias point, keeping the total applied voltage between the collapse and snapback voltages. In this operation regime, the center of the membrane is always in contact with the substrate. Our finite element methods (FEM) calculations reveal that a cMUT operating in this new regime, between collapse and snapback voltages, possesses a coupling efficiency (k_T^2) higher than a cMUT operating in the conventional regime below its collapse voltage. This paper compares the simulation results of the coupling efficiencies of cMUTs operating in conventional and new operation regimes.**

I. Introduction

Capacitive micromachined ultrasonic transducers (cMUTs) were developed as an alternative to piezoelectric transducers [1]–[3]. The cMUTs compete with their piezoelectric counterparts in terms of efficiency and bandwidth [3], [4]. The active part of a cMUT is a metal-coated Si_3N_4 membrane. A highly doped silicon substrate constitutes the bottom electrode. A dc bias voltage applied between the top electrode and the bottom electrode pulls the membrane toward the substrate due to electrostatic attraction. If an ac voltage is applied to a biased membrane, harmonic membrane motion is obtained. The dc bias voltage influences the ac vibration amplitude. As the dc voltage is increased, a larger sinusoidal membrane motion and increase in transmitted power are obtained [5]. Therefore, it is beneficial to operate the cMUT under dc bias close to its collapse voltage. However, the sum of the dc bias and the applied ac signal must be less than the collapse voltage for conventional operation of the cMUT.

If a biased cMUT membrane is subject to an impinging ultrasonic pressure field, the membrane motion generates ac detection currents. This current amplitude increases with increasing bias voltage. The bias voltage can be increased close to the collapse voltage of the membrane to maximize the receive current. Again, it is required that the sum of the bias voltage and the received ac signal is less than the collapse voltage. Therefore, it is difficult to obtain high k_T^2 values with large ac signals in transmit and reception of ultrasonic waves. The transducer's electromechanical coupling efficiency (k_T^2) is a crucial parameter describing the power conversion efficiency of the device. This parameter is, as mentioned, a function of the bias voltage [3]. The electromechanical coupling efficiency k_T^2 increases as the bias voltage increases. For instance, a coupling efficiency exceeding 0.5 requires a bias voltage larger than 90% of the collapse voltage, thus, limiting the maximum applicable ac signal to 10% of the collapse voltage [6].

In this paper, a new regime of operation is proposed. The membrane is first biased at a voltage higher than the collapse voltage, collapsing the membrane onto the substrate. Then, the bias is reduced to a voltage between the collapse and snapback voltages. At this operating voltage, the center of the membrane still contacts the substrate. By adding an ac voltage, harmonic membrane motion is obtained at a circular ring concentric to the center. Our results indicate that the cMUT has a higher electromechanical coupling efficiency in this new regime of operation than that in the conventional precollapse regime.

II. Finite Element Calculations

A typical cMUT features a circular silicon nitride (Si_3N_4) membrane [2]. The membrane is supported at its edges. A vacuum gap is between the membrane and the substrate. A thin insulation layer of Si_3N_4 over the highly doped silicon (Si) substrate prevents shorting the ground electrode and the electrode on the bottom of the membrane at collapse.

Finite element methods (FEM) are used to analyze the cMUT using a commercially available FEM package (ANSYS 5.7, ANSYS Inc., Canonsburg, PA) [7]. The FEM model of a cMUT is shown schematically in Fig. 1. The structure is circularly symmetric allowing the use of 2-D modeling. Boundary conditions have been applied as shown in Fig. 1. The structure is clamped at the symmetry axis in the x-direction to prevent horizontal membrane movement. Moreover, the substrate is supported at the bottom since simulations show that the movement of a 500-μm thick substrate is only 0.1% of the membrane movement. The ground electrode is beneath the Si_3N_4 in-

Manuscript received July 24, 2002; accepted April 29, 2003. This work is supported by the Office of Naval Research. Dr. Hæggström acknowledges the Wihuri-foundation and the Academy of Finland for financial support.

The authors are with the Edward L. Ginzton Laboratory, Stanford University, Stanford, CA 94305-4088 (e-mail: bbayram@stanford.edu).

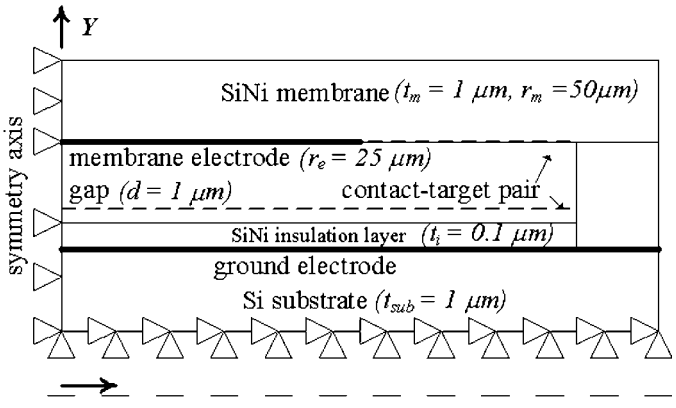

Fig. 1. The cMUT simulation model.

sulation layer. The other electrode is positioned on the bottom surface of the membrane. Its radius (r_e) is half that of the membrane radius, since this has been found optimal for cMUTs for maximum bandwidth [4]. The electrodes are assumed to be infinitesimally thick, which corresponds to 0.2-μm thick electrodes in fabricated devices. This assumption is made since incorporating a thicker electrode only changes the apparent stiffness, not the electrostatics of the membrane. For modeling the membrane substrate contact, FEM elements have been defined on the contacting surfaces as described in the present paragraph.

The ANSYS standard element types, PLANE121, which features charge and voltage variables and PLANE82, which features displacement and force variables, were used for electrostatic and structural analyses, respectively [7]. The collapse of the membrane onto the substrate has been modeled by means of contact-target pair elements (CONTA172 and TARGE169) [7]. These surface contact elements were used to detect contact between the surfaces. The surface elements were defined on the bottom surface of the membrane and slightly above the insulation layer. The offset from the insulation layer was 0.05 μm in the analysis. This offset was required to remesh or remorph the mesh inside the gap when the structure is collapsed.

The FEM was used to calculate the deformed membrane shape for a given bias voltage applied to the membrane electrode. The ground electrode on the substrate was assumed to be at zero potential. First, electrostatic analysis [7] was performed to find the electrostatic forces applied on the membrane. Second, the membrane deformation due to the electrostatic forces was calculated by using structural analysis [7]. When the applied voltage was high, the electrostatic forces deformed the membrane to a great extent, which meant that the electrostatic forces had to be recalculated for the deformed membrane shape. Therefore, the above steps had to be iterated until the equilibrium membrane deflection was reached. The convergence criterion for the simulation was based on the maximum structural displacement, which occurred on the center of the membrane, because convergence determines when the membrane is in its equilibrium position.

When the bias voltage was higher than the collapse voltage, the center of the membrane, with a certain contact radius, collapsed onto the substrate. If the bias voltage was increased further, the contact radius of the collapsed membrane increased. After collapse, calculation of the final membrane shape still required several iterations between electrostatic and structural analyses. Since the maximum displacement was limited by the contact surfaces, the convergence criterion was based on the electrostatic energy after membrane collapse, instead of the maximum structural displacement. When the bias voltage was reduced to a voltage above snapback, the contact radius decreased, and the membrane stayed in contact with the substrate. The contact prevailed until the bias voltage was decreased below the snapback voltage. Therefore, after collapse was reached, reducing the voltage to a reading between collapse and snapback voltages kept the membrane in contact with the substrate.

The emphasis of this paper is the calculation of the coupling efficiency (k_T^2) in this operation regime. Several authors have calculated the coupling efficiency of capacitive transducers. This efficiency, k_T^2, is the ratio of the mechanical energy delivered to the load to the stored total energy in the transducer. Hunt calculated the coupling efficiency for a parallel plate capacitor with a moving electrode [9]. Later, this analysis was extended for circular cMUT membranes by Fraser *et al.* [10]. They calculated k_T^2 for a cMUT membrane using a derivation credited to Berlincourt [11] that relies on the use of the fixed (C^S) and free (C^T) capacitance of the transducer. The fixed capacitance is the capacitance of the transducer at a given dc bias,

$$C^S = C(V)\big|_{V_{DC}}. \tag{1}$$

The free capacitance is defined as

$$C^T = \frac{\mathrm{d}Q(V)}{\mathrm{d}V}\bigg|_{V_{DC}} = \frac{\mathrm{d}}{\mathrm{d}V}\left(VC^S\right)\bigg|_{V_{DC}}, \tag{2}$$

and the coupling efficiency is given by

$$k_T^2 = 1 - \frac{C^S}{C^T}. \tag{3}$$

In this study, FEM was used to extract the fixed capacitance of the final deformed cMUT membrane shape at given bias voltages in order to find the voltage dependence of the capacitance (1). The extraction was done with the predefined function CMATRIX of ANSYS. This function calculated the capacitance using the surface charge distribution on the electrodes. Then, the variable capacitance was calculated using (2).

The mechanical and electrical material properties used in the FEM calculations are given in Table I. The only material parameter required for the electrostatic analysis was the dielectric constant. Structural analysis used Young's modulus, density, and Poisson's ratio. The calculations were performed on a circular membrane as shown in Fig. 1. The membrane radius was 50 μm, while the gap height and the membrane thickness was 1 μm. An insulator layer of 0.1 μm was assumed.

TABLE I
MATERIAL PROPERTIES OF THE MATERIALS USED IN THE SIMULATIONS [8].

	Si_3N_4	Vacuum	Si
Young's Modulus (GPa)	320		169
Poisson's Ratio	0.263		0.721
Density (kg/m^3)	3270		2332
Relative Permittivity	5.7	1	11.8

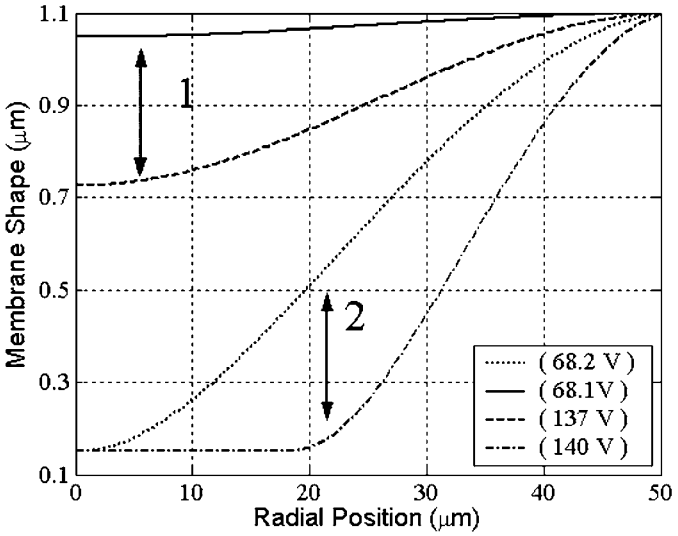

Fig. 2. Membrane shape for different dc bias voltages. The conventional regime of operation is depicted in '1,' and the new regime is depicted in '2.' The arrows indicate membrane motion.

III. RESULTS

The calculated collapse and snapback voltages for the simulated cMUT membrane were 140 V and 68 V, respectively. The calculated membrane shapes for biases in the vicinity of snapback and collapse voltages are depicted in Fig. 2. The arrows indicate the membrane motion.

The vertical axis of the graph shows the position of the bottom surface of the cMUT membrane at each radial distance from the center to the membrane rim. The gap height extends from 0.1 μm, which is the position of the top of the insulation layer, to 1.1 μm, which is the position of the nondeformed membrane with no applied voltage. An increase in the bias voltage results in more membrane deformation. The dashed line in Fig. 2 shows the deformed membrane shape when the applied bias voltage is close to, but still lower than, the collapse voltage. The range between the dashed line and zero displacement indicates the range of motion of the membrane in the conventional regime of operation '1.'

If the applied bias voltage is larger than the collapse voltage, the membrane collapses, and the dash-dot line is obtained. The membrane is in contact with the bottom electrode up to around a radius of 20 μm. As the voltage is reduced, the deformed geometry changes to that of the dotted line in Fig. 2 just before snapback. The contact radius is 2 μm at this instant. The region between the dash-dotted and dotted lines '2' indicates the range of displacement of the deformed membrane while in collapse. The applied voltage can be between 68.2 and 140 V to cause the deformed membrane to move in this new operational regime.

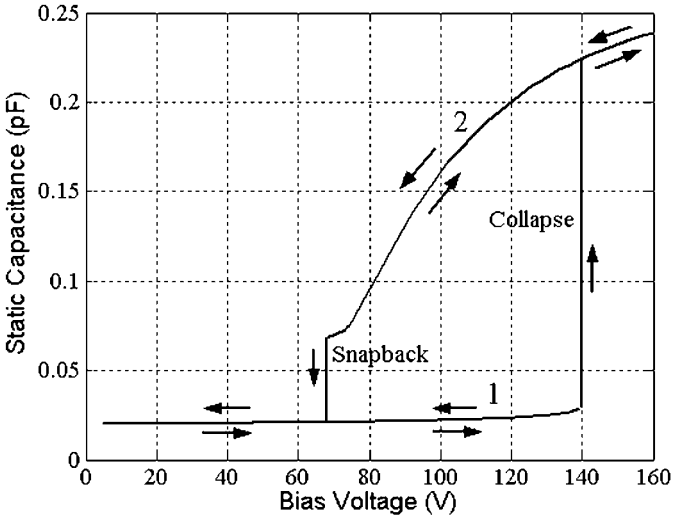

Fig. 3. Simulated voltage-capacitance curve of a cMUT.

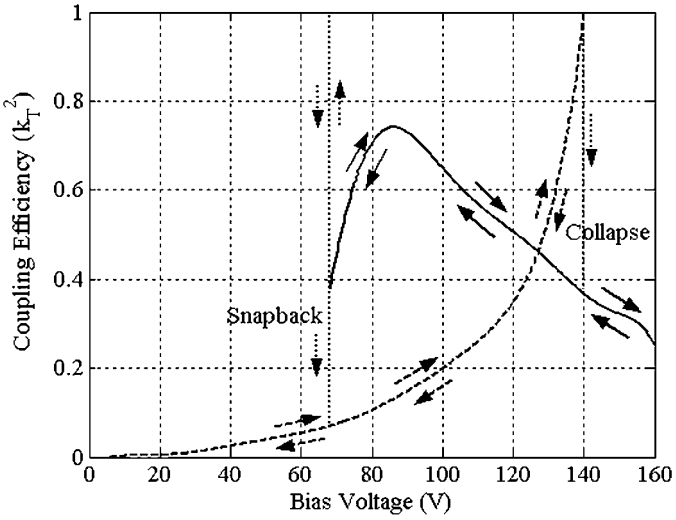

Fig. 4. Simulated coupling efficiency (k_T^2) curve of the model cMUT.

The C^S (V_{DC}) relationship of the modeled cMUT is shown in Fig. 3. The initial static capacitance of 0.020 pF increases to 0.029 pF as the bias voltage is increased close to the collapse voltage. The collapse of the membrane causes an abrupt rise of the static capacitance to 0.22 pF. Subsequently, lowering the bias voltage over the collapsed membrane reduces the static capacitance to 0.07 pF prior to membrane snapback. The static capacitance drops to 0.021 pF when the membrane snaps back.

The electromechanical coupling efficiency (k_T^2) can be calculated using (3). The $k_T^2(V_{DC})$ relationship of the cMUT is given in Fig. 4. The dashed curve is obtained

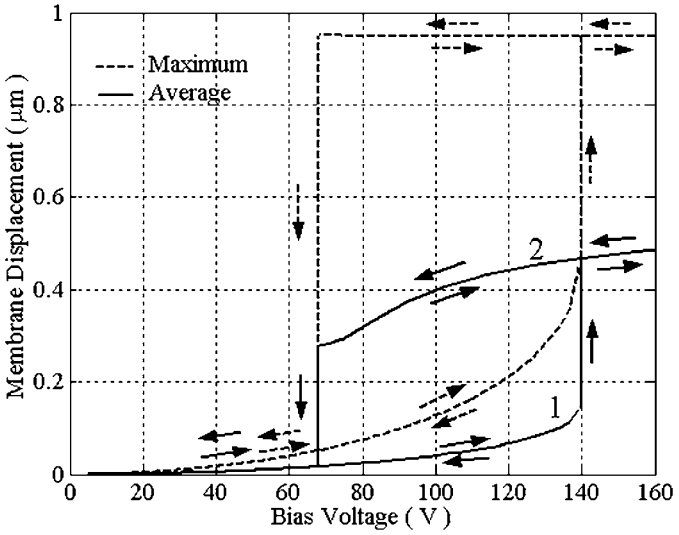

Fig. 5. Simulated average and maximum membrane displacement as a function of applied voltage. The conventional region of operation is depicted in '1,' while the new region of operation is depicted in '2.'

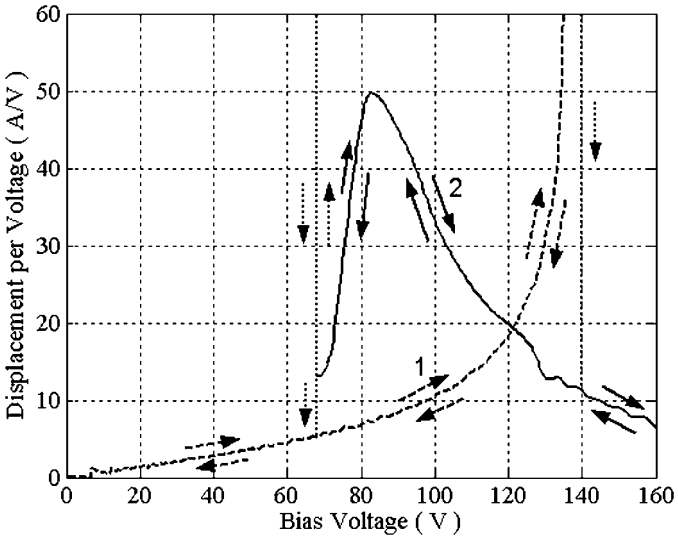

Fig. 6. Average displacement per voltage, for a 1 V ac signal, for the modeled cMUT indicating the sensitivity of the device. The conventional region of operation is depicted in '1,' while the new region of operation is depicted in '2.'

before the membrane collapse. The coupling efficiency k_T^2 increases monotonically to 1 as the bias voltage is increased to collapse voltage. However, as is seen in Fig. 4, a k_T^2 in excess of 0.35 is obtainable only when the bias voltage exceeds 85% of the collapse voltage. If the bias voltage is increased to the collapse voltage, k_T^2 abruptly changes back to 0.35. Further increasing the bias voltage reduces k_T^2 linearly with increased bias voltage. Decreasing the bias voltage after collapsing the membrane increases k_T^2 up to 0.7 at a bias voltage 60% of the collapse voltage. Further decreasing the bias voltage gradually decreases k_T^2 to 0.4 before snapback occurs. Here, the electromechanical coupling efficiency, k_T^2, goes to one at the instant when the state transition takes place and then reduces to 0.07 onto the trace of the curve representing the conventional regime of operation. Thus, a k_T^2 larger than 0.35 is achieved between collapse and snapback voltages with a peak value around 0.7 at a bias voltage 60% of the collapse voltage.

Bias voltage versus average and maximum membrane displacements are shown in Fig. 5. Maximum membrane displacement refers to the displacement of the center of the membrane. Average membrane displacement gives the displacement of an equivalent piston transducer. The average displacement is obtained by averaging the displacement of the FEM elements over the membrane surface. The conventional region of operation is depicted in '1,' and the new region of operation is depicted in '2.' At 100 V dc the average displacement is 0.4 μm in region '2' compared with 0.15 μm in region '1.' The change in average displacement in region '2' is 0.19 between dc voltages from 68 V to 140 V, while the change in average displacement in region '1' is 0.11.

The voltage derivative of the average membrane displacement, shown in Fig. 6, gives the displacement per volt curve, i.e., the output displacement (transmitter) capability of the transducer. A maximum displacement of

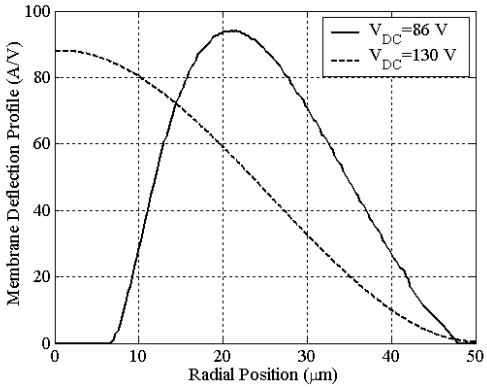

Fig. 7. Simulated membrane deflection profile of a noncollapsed and of a collapsed membrane using a 1 V ac signal.

50 Å/V_{AC}, is obtained at 86 V_{DC}. For V_{DC} values between 78 V and 95 V the output displacement is larger than 40 Å/V.

The details of the membrane displacement in the noncollapsed and collapsed modes of operation are shown in Fig. 7. In the noncollapsed mode, a dc bias of 130 V and an ac signal of 1 V cause the displacement profile shown with the dashed line. A peak displacement of 90 Å is obtained in the center of the membrane. The displacement gradually reduces to zero at membrane edge. In the new operation regime, a dc bias of 86 V (k_T^2 = 0.75, cfr. Fig. 4.) and an ac signal of 1 V cause the displacement profile shown with the solid line. The displacement is zero at the center and at the membrane edge but has a peak displacement of 95 Å, cfr. Fig. 5, at around half the membrane radius. The excited mode can be seen as the first-order mode of the ring shape.

IV. Discussion

Following is a discussion of the assumptions underlying the simulation and their implications on obtained results. In addition, we consider the relevance of the obtained simulation results with respect to device fabrication.

The traditional k_T^2 calculation for a PZT transducer is performed in a quasi-static manner. Berlincourt calculated k_T^2 for a piezo-transducer using the relation between the applied electric field and the induced electrical displacement field. For a piezoelectric device, the permittivity of a clamped and a free ceramic are different. The difference is due to energy stored in the device [11]. This same approach was used by Fraser to calculate the stored and the available energy in a capacitive device. For a capacitive device the charge—voltage relation is used instead of the electric field—electric displacement field used for a piezoelectric ceramic. In a capacitive device the free and the clamped capacitance of the device also differ [10].

Consider a capacitive device where one part is free to move. A dc source is connected to the device and as the dc voltage is increased to a certain point, electrical energy is stored in the device. Then, the moving part is clamped and as the dc voltage is decreased to zero a certain amount of energy is still stored in the device. The difference between these two amounts of energy in the device, regardless of their spatial distribution, is per definition the stored energy in the device. This stored energy is therefore not available to the source.

Then, the ratio of the energy available to the load divided by the total energy in the device is defined as k_T^2. Therefore, as long as the capacitance of the device is calculated taking into account the device geometry, the used k_T^2 calculation is valid both for parallel plates and for membranes with curvature. The details of our k_T^2 calculation can be found in [12]. In the paper it is shown, using FEM relying on Fraser's calculations (using the ratio of converted energy to stored energy), that k_T^2 of a circular cMUT asymptotically approaches unity as the dc bias approaches collapse voltage. These calculations, based on small relative changes in the applied E-field, contain at each step the displacement shape, thus implicitly taking into account the energy distribution of the membrane.

Eq. (2) is derived for a capacitor the geometry of which is known. It relies on knowing the V-Q (voltage-charge) curve of the device. The only assumption made is that of small relative changes in E-field between the modeling steps since the tangent of the V-Q curve is used. This requirement was fulfilled in our simulations since we always used less than 0.1% relative E-field changes between the modeling steps. Eq. (3) states the geometrical relationship between the converted energy and the stored energy in terms of free and static capacitance and does not contain additional assumptions.

One of the assumptions implicitly present in this work is that ac parameters, e.g., k_T^2 can be obtained from dc parameters, such as voltage-capacitance and voltage-deflection relations. This assumption is supported by the theoretical work cited in [9]–[11]. The reason why dc parameters can be used to derive ac parameters is that a small signal approximation can be used since the incremental dc steps are small. Another artificial feature in the FEM model of the cMUT is the offset. This feature does not change the overall response of the cMUT, but it increases the equivalent insulation thickness and thus changes the snapback voltage.

Another assumption is that infinitesimally thick electrodes should not alter the results significantly as long as the electrostatic solution is fairly constant with electrode thickness. An increased electrode thickness will in practice only change the apparent stiffness of the membrane.

There are several interesting features present in Fig. 2 to 7. In Fig. 2, the membrane can deform and thus emit sound, even if it is collapsed. In the conventional regime, '1,' the volumetric change (11%) is approximately half of that in the new regime, '2' (19%). Considerable volume displacement can be achieved in this operation.

In Fig. 2, the simulated structure with a 0.1-μm insulation layer and 0.05-μm offset in the 1-μm gap corresponds to a structure with a 0.38-μm insulation layer and a 0.95-μm gap with no offset. This is due to the permittivity of the insulation layer, 5.7, compared with 1.0 for the vacuous gap.

Fig. 3 indicates how the device can be operated. It is seen that in the conventional regime of operation, the capacitance change with applied voltage is small compared with operation in the new regime. In the new regime, both the static capacitance (ordinate) and the variation in the static capacitance (slope of the static capacitance curve) increase. Increase in the variation of the static capacitance is larger than the increase in the static capacitance thus increasing k_T^2 compared with operation in the conventional regime between 68 V and 130 V bias. Most important is that the ratio of dynamic to static capacitance, averaged over bias voltages 68 V and 140 V, increases from 0.32 to 0.97. This translates directly into sensitivity of the cMUT operating as a receiver.

The parasitic capacitance is the fraction of the device capacitance that cannot be modulated by membrane vibration of a cMUT. The main contribution to the parasitic capacitance in the classical regime of operation stems from the edges of the membranes that move less than the center of the membrane. In region '1,' the parasitic capacitance is generally less than 10% of the total capacitance of the membrane [13]. Moreover, k_T^2 is reduced since the parasitic capacitance is increased in this region [13]. In regime '2,' the main contribution to the parasitic capacitance is probably from the contact region. The parasitic capacitance should therefore increase with increased bias voltage. Furthermore, this insight implies that it might be useful to use a partial metallization where the center of the membrane is not metallized.

In Fig. 4, it is seen that with a bias voltage smaller than the collapse voltage, it is possible to obtain high k_T^2 values. This makes it possible to use large ac signals without risk of collapse. Small changes in bias voltage only slightly

change the k_T^2 value thus making the output power more predictable. When V_{DC} is 75 to 105 V, k_T^2 is 0.6 to 0.75. Also, in order to obtain k_T^2 values above those obtained in region '2,' the ac signal is limited to 5% of the collapse voltage. Moreover, the average k_T^2 value for a large ac signal (100 ± 30 V) is 0.3 in region '1' and 0.6 in regime '2.' This constitutes an increase of 100%, which is advantageous, both when the cMUT is used as a receiver and as a transmitter.

We do not have an expression for large amplitude ac signals. Fig. 4 should, however, be indicative of the device performance with large amplitude ac signals. The reason is that (2) is valid for any known capacitor geometry and relies only on the V-Q curve of the device and on the assumption of small relative changes in E-field between the modeling steps. This requirement was fulfilled in our simulations since we always used less than 0.1% relative E-field changes between the modeling steps.

From Fig. 5 that does not carry the small-signal approximation present in Fig. 6, we get average membrane displacement even though the maximum displacement is bounded with the contacting surfaces. The maximum displacement curve is clamped at 0.95 μm, while the average displacement curve changes from 0.25 to 0.45 μm, which is to be compared with 0.05 to 0.15 μm for region '1.' This translates into a four times larger output power, which is of benefit when the cMUT operates as a transmitter. Fig. 6 shows the benefits of operating the device in the new regime compared with operating it in the conventional regime. In another paper, we will describe collapse-snapback cycle operation obtained by moving between '1' and '2.'

In Fig. 6, it is seen that a larger displacement (50 Å/V) and increased output power ($\sim$displacement^2) is obtained while operating in the new proposed regime, as compared with the conventional regime (10 Å/V at the same bias voltage). In Figs. 5 and 6 a high k_T^2 also corresponds to a large displacement of the moving membrane. The local maximum of this small-signal curve indicates a preferable point of operation providing large displacement with no risk of snapback. This point of operation gives a displacement corresponding to that obtained by operating at a bias voltage that is larger than 95% of the collapse voltage. By applying 1 V ac and 86 V dc, one gets 50 Å average displacement, while in the conventional regime, by applying 1 V ac and 130 V dc, one gets 30 Å average displacement. In Figs. 5 and 6 we get increased sensitivity (displacement/V ac) as increased total peak pressure by using the new regime in comparison with using the conventional regime.

In Fig. 7, operating the cMUT in the new regime alters the mode shape of the membrane from the first mode of the circle to the first mode of a ring membrane. This might imply an increase in the fundamental resonance frequency since the center of the membrane is collapsed onto the substrate, making the vibrating structure smaller.

Finally, it is not yet clear how the bandwidth (BW) will change as the cMUT is operated in the new regime. In principle, the fractional BW is proportional to k_T^2 [3], [4]. Since Fig. 4 shows increasing k_T^2 with decreasing bias in the new regime of operation, it is plausible that the fractional BW increases. Fig. 2 shows larger vibrating structures with decreasing bias, implicating lower resonance frequency. Although the resonance frequency decreases with decreased bias, it is still larger than the resonance frequency obtained in the conventional region. This implies that operating the cMUT in the new regime could increase the bandwidth of the cMUT. This is currently a topic of investigation.

For piezoelectric transducers, the transducer properties, such as bandwidth and sensitivity, are dictated by the quasi-static k_T^2. This should, by implication, be the case cMUT transducers, too since, the equivalent circuits used to describe both these device classes are identical. Caronti *et al.* [14], on the other hand, calculates the k_T^2, at resonance, using dynamic modeling. It is, however, not clear how this k_T^2 value is related to the bandwidth of the modeled device.

In summary, the obtained simulation results indicate that operating the cMUT in the new regime both in transmit and receive mode could be beneficial. The results also indicate that an increase in sensitivity, peak output pressure, and in total acoustic energy transmitted could be obtained by operating the transducer in the new regime compared with operating in the conventional regime.

V. Conclusions

High coupling efficiency (k_T^2) traditionally requires the bias of a cMUT to be close to the collapse voltage of its membrane. However, a collapsed membrane has been shown to feature a high coupling efficiency (k_T^2) between collapse and snapback voltages. Membrane displacement curves suggest that higher acoustic pressures could be generated in this mode compared with operation in the classic regime. A new operation regime for a collapsed membrane may thus be beneficial in the design of future generation cMUTs.

References

[1] M. I. Haller and B. T. Khuri-Yakub, "A surface micromachined electrostatic ultrasonic air transducer," in *Proc. IEEE Ultrason. Symp.*, 1994, pp. 1241–1244.

[2] H. T. Soh, I. Ladabaum, A. Atalar, C. F. Quate, and B. T. Khuri-Yakub, "Silicon micromachined ultrasonic immersion transducers," *Appl. Phys. Lett.*, vol. 69, pp. 3674–3676, Dec. 1996.

[3] I. Ladabaum, X. Jin, H. T. Soh, A. Atalar, and B. T. Khuri-Yakub, "Surface micromachined capacitive ultrasonic transducers," *IEEE Trans. Ultrason., Ferroelect., Freq. Contr.*, vol. 45, no. 3, pp. 678–690, May 1998.

[4] A. Bozkurt, A. Atalar, and B. T. Khuri-Yakub, "Theory and analysis of electrode size optimization for capacitive microfabricated ultrasonic transducers," *IEEE Trans. Ultrason., Ferroelect., Freq. Contr.*, vol. 46, no. 6, pp. 1364–1374, Nov. 1999.

[5] A. S. Ergun, B. Temelkuran, E. Ozbay, and A. Atalar, "A new detection method for capacitive micromachined ultrasonic transducers," *IEEE Trans. Ultrason., Ferroelect., Freq. Contr.*, vol. 48, no. 4, pp. 932–942, July 2001.

[6] P. C. Eccardt and K. Niederer, "Micromachined ultrasonic transducers with improved coupling factors from a CMOS compatible process," *Ultrasonics*, vol. 38, pp. 774–778, 2000.
[7] ANSYS 5.7, Ansys Inc., Canonsburg, PA.
[8] B. Auld, *Acoustic Fields and Waves in Solids*. 2nd ed. Malabar, FL: R. E. Krieger Publishing, 1990.
[9] F. V. Hunt, *Electroacoustics; the analysis of transduction, and its historical background*. Cambridge: Harvard University Press, 1954, pp. 181–187.
[10] J. Fraser and P. Reynolds, "Finite-element method for determination of electromechanical coupling coefficient for piezoelectric and capacitive micromachined ultrasonic transducers," presented at Joint 140th meeting of ASA/NOISE-CON, 2000.
[11] D. Berlincourt, "Piezoelectric crystals and ceramics," in *Ultrasonic Transducer Materials*. O. E. Mattiat, Ed. New York: Plenum Press, 1971, pp. 69–71.
[12] G. G. Yaralioglu, A. S. Ergun, B. Bayram, E. Hæggström, and B. T. Khuri-Yakub, "Calculation and measurement of electromechanical coupling coefficient of capacitive micromachined ultrasonic transducers," *IEEE Trans. Ultrason., Ferroelect., Freq. Contr.*, vol. 50, no. 4, pp. 449–456, Apr. 2003.
[13] P. C. Eccardt, K. Niederer, and B. Fischer, "Micromachined transducers for ultrasound applications," in *Proc. IEEE Ultrason. Symp.*, 1997, pp. 1609–1618.
[14] A. Caronti, R. Carutenuto, and M. Pappalardo, "Electromechanical coupling factor of capacitive micromachined ultrasonic transducers," *J. Acoust. Soc. Amer.*, vol. 113, no. 1, pp. 279–288, Jan. 2003.

Baris Bayram was born in Izmir, Turkey. He received the B.S. degree in 2000 from Bilkent University, Ankara, Turkey and the M.S. degree in 2002 from Stanford University, Stanford, CA, both in electrical engineering. He is currently a Ph.D. candidate at the E. L. Ginzton Laboratory of Stanford University and his current research interests include the modeling, simulation, fabrication, and experimental characterization of capacitive micromachined ultrasonic transducers for low voltage and reduced crosstalk operation.

Edward Hæggström is a visiting scholar at Ginzton Lab (Khuri-Yakub group), Stanford University, Stanford, CA, on leave from his position as assistant professor at the Department of Physics at the University of Helsinki. He received his D.Sc. degree in 1998 in applied physics from the University of Helsinki, Finland and an MBA in innovation management from the Helsinki University of Technology in 2001. His principal research interests are within ultrasonic characterization of biological samples.

Goksen Goksenin Yaralioglu (S'92–M'99) was born in Akhisar, Turkey on May 13, 1970. He received his B.S., M.S. and Ph.D. degrees from Bilkent University, Ankara, Turkey, in 1992, 1994, and 1999, respectively, all in electrical engineering. He is now working as an engineering research associate in E.L. Ginzton Laboratory, Stanford University, Stanford, CA. His current research interests include design, modeling, and applications of micromachined ultrasonic transducers, and atomic force microscopy at ultrasonic frequencies.

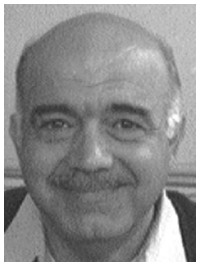

Butrus T. Khuri-Yakub (S'70–S'73–M'76–SM'87–F'95) was born in Beirut, Lebanon. He received the B.S. degree in 1970 from the American University of Beirut, the M.S. degree in 1972 from Dartmouth College, and the Ph.D. degree in 1975 from Stanford University, Stanford, CA, all in electrical engineering. He joined the research staff at the E. L. Ginzton Laboratory of Stanford University in 1976 as a Research Associate. He was promoted to Senior Research Associate in 1978, and to Professor of Electrical Engineering (Research) in 1982. He has served on many university committees in the School of Engineering and the Department of Electrical Engineering.

Presently, he is the Deputy Director of the E. L. Ginzton Laboratory. Professor Khuri-Yakub has been teaching both at the graduate and undergraduate levels for more than 15 years, and his current research interests include *in situ* acoustic sensors (temperature, film thickness, resist cure,etc.) for monitoring and control of integrated circuits manufacturing processes, micromachining silicon to make acoustic materials and devices such as airborne and water immersion ultrasonic transducers and arrays, and fluid ejectors, and in the field of ultrasonic nondestructive evaluation and acoustic imaging and microscopy.

Professor Khuri-Yakub is a fellow of the IEEE, a senior member of the Acoustical Society of America, and a member of Tau Beta Pi. He is associate editor of *Research in Nondestructive Evaluation*, a journal of the American Society for Nondestructive Testing. Professor Khuri-Yakub has authored more than 300 publications and has been principal inventor or co-inventor of 52 issued patents. He received the Stanford University School of Engineering Distinguished Advisor Award, June 1987 and the Medal of the City of Bordeaux for contributions to NDE, 1983.